Spectral phase, amplitude, and spatial modulation from ultraviolet to infrared with a reflective MEMS pulse shaper

Jérôme Extermann,[1] **Stefan M. Weber,**[1,2] **Denis Kiselev,**[1] **Luigi Bonacina,**[1,*] **Sébastien Lani,**[2] **Fabio Jutzi,**[2] **Wilfried Noell,**[2] **Nico F. de Rooij,**[2] **and Jean-Pierre Wolf**[1]

[1]*GAP-Biophotonics, Université de Genève, 20 rue de l'Ecole de Médecine, 1211 Genève 4, Switzerland*

[2]*École Polytechnique Fédérale de Lausanne/STI/IMT-NE/SAMLAB, Rue Jaquet-Droz 1, 2002 Neuchâtel, Switzerland*

**luigi.bonacina@unige.ch*

Abstract: We describe the performance of a reflective pulse-shaper based on a Micro-ElectroMechanical System (MEMS) linear mirror array. It represents a substantial upgrade of a preceding release [Opt. Lett. **35**, 3102 (2010)] as it allows simultaneous piston and tilt mirror motion, allowing both phase- and binary amplitude-shaping with no wavelength restriction. Moreover, we show how the combination of in-axis and tilt movement can be used for active correction of spatial chirp.

OCIS codes: (230.4040) Optical devices; (230.4685) Optical microelectromechanical devices; (320.2250) Femtosecond phenomena; (320.5540) Pulse shaping.

References and links

1. A. Assion, T. Baumert, M. Bergt, T. Brixner, B. Kiefer, V. Seyfried, M. Strehle and G. Gerber, "Control of chemical reactions by feedback-optimized phase-shaped femtosecond laser pulses," Science **282**, 919–922 (1998).
2. D. Meshulach and Y. Silberberg, "Coherent quantum control of two-photon transitions by a femtosecond laser pulse," Nature **396**, 239–242 (1998).
3. T. Brixner, N. H. Damrauer, P. Niklaus and G. Gerber, "Photoselective adaptive femtosecond quantum control in the liquid phase," Nature **414**, 57–60 (2001).
4. M. Dantus and V. V. Lozovoy, "Experimental coherent laser control of physicochemical processes," Chem. Rev. **104**, 1813–1859 (2004).
5. M. Roth, L. Guyon, J. Roslund, V. Boutou, F. Courvoisier, J. P. Wolf, and H. Rabitz, "Quantum control of tightly competitive product channels," Phys. Rev. Lett. **102**, 253001 (2009).
6. A. M. Weiner, "Femtosecond pulse shaping using spatial light modulators," Rev. Sci. Instrum. **71**, 1929–1960 (2000).
7. A. M. Weiner, J. P. Heritage, and E. M. Kirschner, "High-resolution femtosecond pulse shaping," J. Opt. Soc. Am. B **5**, 1563–1572 (1988).
8. T. Tanigawa, Y. Sakakibara, S.B. Fang, T. Sekikawa, and M. Yamashita, "Spatial light modulator of 648 pixels with liquid crystal transparent from ultraviolet to near-infrared and its chirp compensation application," Opt. Lett. **34**, 1696–1698 (2009).
9. S. Coudreau, D. Kaplan, and P. Tournois, "Ultraviolet acousto-optic programmable dispersive filter laser pulse shaping in KDP," Opt. Lett. **31**, 1899–1901 (2006).
10. B. J. Pearson and T. C. Weinacht, "Shaped ultrafast laser pulses in the deep ultraviolet," Opt. Express **15**, 4385–4388 (2007).
11. S. Weber, M. Barthelemy, and B. Chatel, "Direct shaping of tunable UV ultra-short pulses," Appl. Phys. B **98**, 323–326 (2010).
12. N. Krebs, R. A. Probst, and E. Riedle, "Sub-20 fs pulses shaped directly in the UV by an acousto-optic programmable dispersive filter," Opt. Express **18**, 6164–6171 (2010).

#142090 - $15.00 USD Received 3 Feb 2011; revised 17 Mar 2011; accepted 17 Mar 2011; published 5 Apr 2011

13. M. Hacker, G. Stobrawa, R. Sauerbrey, T. Buckup, M. Motzkus, M. Wildenhain, and A. Gehner, "Micromirror SLM for femtosecond pulse shaping in the ultraviolet," Appl. Phys. B **76**, 711–714 (2003).
14. A. Rondi, J. Extermann, L. Bonacina, S. M. Weber, and J. P. Wolf, "Characterization of a mems-based pulse-shaping device in the deep ultraviolet," Appl. Phys. B **96**, 757–761 (2009).
15. J. Mohring, T. Buckup, C. S. Lehmann, and M. Motzkus, "Generation of phase-controlled ultraviolet pulses and characterization by a simple autocorrelator setup," J. Opt. Soc. Am. B **26**, 1538–1544 (2009).
16. S. M. Weber, J. Extermann, L. Bonacina, W. Noell, D. Kiselev, S. Waldis, N. F. Rooij, and J. P. Wolf, "Ultraviolet and near-infrared femtosecond temporal pulse shaping with a new high-aspect-ratio one-dimensional micromirror array," Opt. Lett. **35**, 3102–3104 (2010).
17. S. M. Weber, W. Noell, D. Kiselev, F. Extermann, S. Lani, L. Bonacina, J. P. Wolf, and N. F. Rooij, "Design, simulation, fabrication, packaging, and characterization of mems micromirror array for femtosecond pulse shaping in amplitude and phase," submitted to Rev. Sci. Instrum.
18. O. E. Martinez, "Grating and prism compressors in the case of finite beam size," J. Opt. Soc. Am. B **3**, 929–934 (1986).
19. S. Linden, J. Kuhl, and H. Giessen, "Amplitude and phase characterization of weak blue ultrashort pulses by downconversion," Opt. Lett. **24**, 569–571 (1999).
20. R. Trebino, K. W. DeLong, D. N. Fittinghoff, J. N. Sweetser, M. A. Krumbugel, B. A. Richman, and D. J. Kane, "Measuring ultrashort laser pulses in the time-frequency domain using frequency-resolved optical gating," Rev. Sci. Instrum. **68**, 3277–3295 (1997).
21. M. M. Wefers and K. A. Nelson, "Analysis of programmable ultrashort wave-form generation using liquid-crystal spatial light modulators," J. Opt. Soc. Am. B **12**, 1343–1362 (1995).
22. P. Baum, S. Lochbrunner, and E. Riedle, "Generation of tunable 7 fs ultraviolet pulses: achromatic phase matching and chirp management," Appl. Phys. B **79**, 1027–1032 (2004).
23. D. Oron, E. Tal, and Y. Silberberg, "Scanningless depth-resolved microscopy," Opt. Express **13**, 1468–1476 (2005).
24. T. Feurer, J. C. Vaughan, R. M. Koehl, and K. A. Nelson, "Multidimensional control of femtosecond pulses by use of a programmable liquid-crystal matrix," Opt. Lett. **27**, 652–654 (2002).
25. M. M. Wefers and K. A. Nelson, "Space-time profiles of shaped ultrafast optical waveforms," IEEE J. Quantum Electron. **32**, 161–172 (1996).
26. B. J. Sussman, R. Lausten, and A. Stolow, "Focusing of light following a 4-f pulse shaper: Considerations for quantum control," Phys. Rev. A **77**, 043416 (2008).
27. F. Frei, A. Galler, and T. Feurer, "Space-time coupling in femtosecond pulse shaping and its effects on coherent control," J. Chem. Phys. **130**, 034302 (2009).
28. S. Akturk, X. Gu, P. Bowlan, and R. Trebino, "Spatio-temporal couplings in ultrashort laser pulses," J. Opt. **12**, 093001 (2010).

1. Introduction

Research and industrial interest towards coherent large bandwidth sources is steadily increasing. Their appeal primarily comes from their versatility: large bandwidth pulses, which are associated to short time duration, nowadays as low as 10 fs even for commercial turn-key systems, are paramount ingredients in nonlinear optics, spectroscopy, and imaging. Thanks to their high peak powers (GW to TW), these pulses can easily induce nonlinear effects using comparatively low energies (pJ to mJ). Moreover, their ultrashort duration is exploited for studying and controlling molecular and material processes on a sub-picosecond timescale. All these applications can further profit from a tailored manipulation of the spectral and temporal properties of the pulses [1–5], which has motivated the development of pulse-shaping theory and the parallel evolution of pulse-shaping devices [6]. Presently, the latter are dominated by liquid crystal arrays which have proven very reliable [7]. Their main limitation is the material transmission cut-off in the visible-UV region, an issue only recently addressed by the group of Yamashita [8]. Acousto-optic modulators are an interesting alternative, as they are characterized by very easy alignment and operation. An opportune choice of the active crystal allows employing them in the UV spectral region [9, 10]. However, these positive features are downturned by their low throughput, limited bandwidth acceptance, and damage threshold [11,12]. A third option, which remains quite overlooked at the moment, is represented by Micro-ElectroMechanical System (MEMS)-based all-reflective shapers. The use of MEMS mirror arrays for temporal pulse-shaping was firstly proposed by Hacker *et al*. in 2003 using a two-dimensional device [13].

#142090 - $15.00 USD Received 3 Feb 2011; revised 17 Mar 2011; accepted 17 Mar 2011; published 5 Apr 2011

Subsequently, a series of characterizations of the same chip have been carried out by ours [14] and by the Motkus research group [15] at 266 and 315 nm, respectively. Very recently, we have described the performances of a novel one-dimensional MEMS device for phase-only shaping that we designed and developed. We applied linear and quadratic phase modulations demonstrating the temporal compression of 800 and 400 nm pulses [16].

In this contribution, we present a substantial upgrade of this device, as we have added to piston motion (phase-shaping) the additional possibility of mirror tilting. As we demonstrate in the following, this operation allows simultaneous phase- and (binary) amplitude-shaping. In the last section, we discuss other prospective and yet unexplored possibilities opened by this additional degree of freedom in terms of combined phase- and spatial-shaping. The present paper, which illustrates the optical implementation and characterization of our new device is complemented by a technical manuscript, which describes in full details the MEMS chip design, actuation, and electronics [17].

2. Experimental

2.1. Optical setup

A detailed scheme of the set-up can be found in Ref. [16]. The laser source is a 17 femtosecond (fs) oscillator (Femtolaser, Femtosource Synergia 20) frequency doubled at 400 nm in a 150-μm-thick beta barium borate (BBO) crystal. The beam diameter is adjusted to 1 mm diameter to best match the vertical dimensions of the mirror elements of the MEMS device. The latter is placed at the Fourier plane of a folded, 4-f dispersion-free compressor [18] constituted of a 1200 grooves/mm and a f =150 mm cylindrical lens. The resulting spectrum is dispersed over the whole working section of the device with a full width at half maximum of 1.85 mm (Gaussian fit). The spatial characterization of the shaped beam is realized by a Newport LBP-1 profiler. The spectra at 400 nm are acquired by an in-line CCD array (Thorlabs LC1-USB) placed at the imaging output port of a spectrometer (Princeton Instruments, Acton, SP2300i). Cross FROG (XFROG) traces [19, 20] are realized by frequency mixing the shaped 400 nm pulses with a portion of the fundamental 800 nm laser output in a 100-μm-thick BBO. The sum frequency signal at 266 nm is detected by a photomultiplier placed at the slit output of the spectrometer as a function of the relative time-delay between the 400 and 800 nm pulses, realized by varying the 800 nm optical path by means of a high-resolution linear translation stage (Physik Instrumente, M-505).

2.2. MEMS device

A throughout description of the MEMS chip and driving electronics is given in the accompanying technical paper [17]. The device is bulk-micromachined from a silicon-on-insulator wafer with a 35-μm-thick device layer using delayed-mask deep reactive ion etching. Because of the limited yield of the first production run, we could address only a limited region of 26 mirrors with the prototype chip used in this work. The size of each of these aluminum coated mirrors is 160×1000 μm^2 and, accounting for the 3 μm inter-mirrors gaps, the overall fill factor is greater than 98%. A single mirror element features independent actuators for tilt and piston, which are connected to the outer edges via X shaped springs, optimized to produce a viable compromise between stability and the specified angle and piston motions. Both degrees of freedom are enacted using a single spring: vertical comb drives are used in a symmetric way for out-of-plane piston movement, and in an asymmetric manner for enacting the torque for tilting. For the maximally applied voltage of 100 V, the piston stroke is 2.5 μm and the mechanical tilt 0.67 deg, corresponding to 1.3 deg of actual optical deflection.

#142090 - $15.00 USD Received 3 Feb 2011; revised 17 Mar 2011; accepted 17 Mar 2011; published 5 Apr 2011

3. Results and discussion

3.1. Spectral separation and amplitude shaping

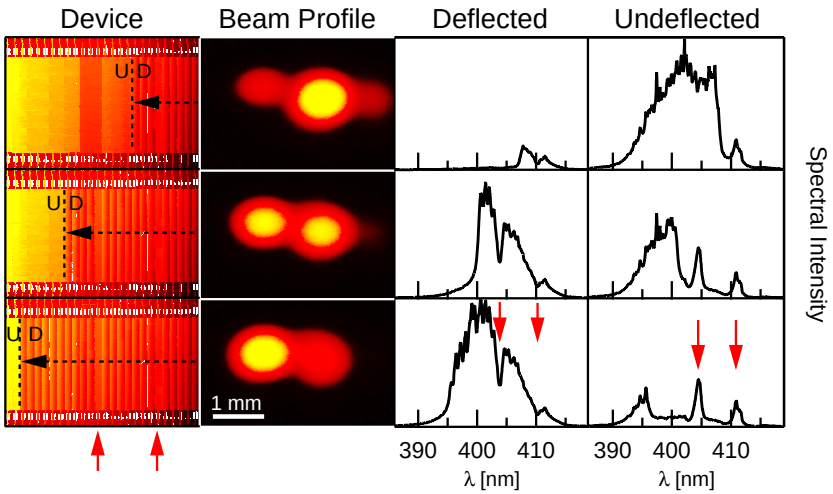

Fig. 1. (Media 1) Spectral amplitude modulation. First column: white-light interferometry profile of the MEMS device region addressed. The horizontal dashed lines indicate the deflected (*D*) and undeflected (*U*) mirrors in the three different cases corresponding to the three rows: 9 (first row), 18 (second row), and 24 (third row) mirrors in the deflected state. The vertical arrows indicate the position of the two nonworking mirrors. Second column: output beam profile measured for the different MEMS actuation conditions. Third and fourth column: spectral intensity acquired for the deflected and undeflected beam, respectively. The two red arrows indicate the spectral position of the two nonworking mirrors.

In a first series of measurements, summarized in Fig. 1, we have thoroughly examined the effect of individual mirror tilting on the spatial and spectral properties of the beam. The interferometric images of the device shown in the leftmost column, indicate the actuation state of the device: 9, 18, and 24 neighboring mirrors out of 26 are deflected for the measurements presented in the first, second, and third row, respectively. All mirrors except two defective ones that could not be actuated (indicated by the red arrows), were mechanically tilted by 0.4 deg around a vertical axis parallel to the Fourier plane. As shown by the beam profiles in the second column, after the shaper grating the back-reflected beam is comprised by two parallel components horizontally displaced by $\sim$ 1 mm. The spectral components associated to each of these two portions are shown in the two rightmost columns. An animated version of the same picture is provided as online supplementary material. Given the good separation and excellent profile quality, mirror tilting can be used for binary spectral amplitude modulation by spatially selecting with a diaphragm one of the two beams. The intensity contrast observed is $\sim$ 90%. In a standard $4-f$ set-up, the ultimate spectral resolution is determined by the interplay between mirror lateral size, grating period, and horizontal dimension of the sagittal beam focused spot [6].

To demonstrate time-domain pulse-shaping by amplitude modulation, in Fig. 2(A) we present the effect of imposing a regular binary actuation pattern on the spectrum of the deflected beam portion, by tilting by 0.4 deg every second mirror in the array. Figure 2(B) corresponds to the result obtained by applying the complementary mask. According to shaping theory, such a regular spectral modulation corresponds to a multiple-pulse structure in the time-domain with a pulse-separation inversely proportional to the spectral modulation frequency. Indeed, the XFROG

#142090 - $15.00 USD Received 3 Feb 2011; revised 17 Mar 2011; accepted 17 Mar 2011; published 5 Apr 2011

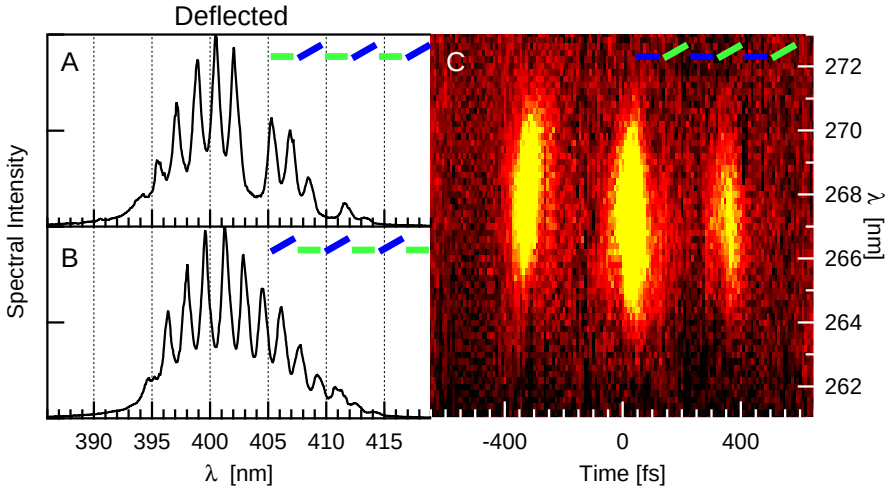

Fig. 2. Time-domain modulation by amplitude shaping. Spectra recorded for the deflected beams when every even (A) or odd (B) mirror is tilted. (C) Typical XFROG resulting from applying an alternating tilted/untilted mirror pattern. In the symbolic mirrors representations in the top right corners of the plots, the blue elements correspond to the observed beam portion in the plots.

trace in panel C, corresponds to that of two femtosecond pulses delayed by ~ 350 fs.

3.2. Phase-shaping

As extensively described in our previous publication [16], temporal shaping of femtosecond pulses is obtained by imposing variable phase-shifts on selected spectral components by offsetting the mirror positions with respect to the Fourier plane. In the same work, we addressed a series of phase-shaping examples, including correction of positive and negative temporal chirp. Here, we focus on the unique features of our piston/tilt device, which, quite notably, allows simultaneous piston and tilt actuation of individual mirrors, enabling the possibility to impose independent phase-shifts on both the un-deflected and deflected spectral components. In Fig. 3, we show two exemplary cross-correlation traces obtained for the rather extreme situation of two isolated spectral portions interfering in the time-domain. Panel A displays the trace obtained for the undeflected beam portion for two different phase-shifts between two spectral components set 3.3 nm apart (solid line $\Delta\phi = 0$, dotted line $\Delta\phi = \pi$). The results of the same procedure applied on the deflected beam are illustrated in Fig. 3(B). The dashed dotted curve super-imposed to both plots correspond to the theoretical pulse shaping window, indicating the expected intensity of a phase-shaped pulse as a function of time [21].

3.3. Spatial chirp

A highly undesirable effect often encountered when working with large bandwidth femtosecond pulses is spatial chirp, i.e. the fact that different frequency components are separated in a plane orthogonal to the propagation direction. Such a situation sets in, for instance, after transmission trough a tilted substrate, after propagation through a prism or grating compressor, or after frequency conversion in a nonlinear crystal. In some defined contexts, these effects can be quantified and compensated for by a clever design of the optical system: for example pulse compressors comprise of four passages through angularly dispersive elements at this scope.

#142090 - $15.00 USD Received 3 Feb 2011; revised 17 Mar 2011; accepted 17 Mar 2011; published 5 Apr 2011

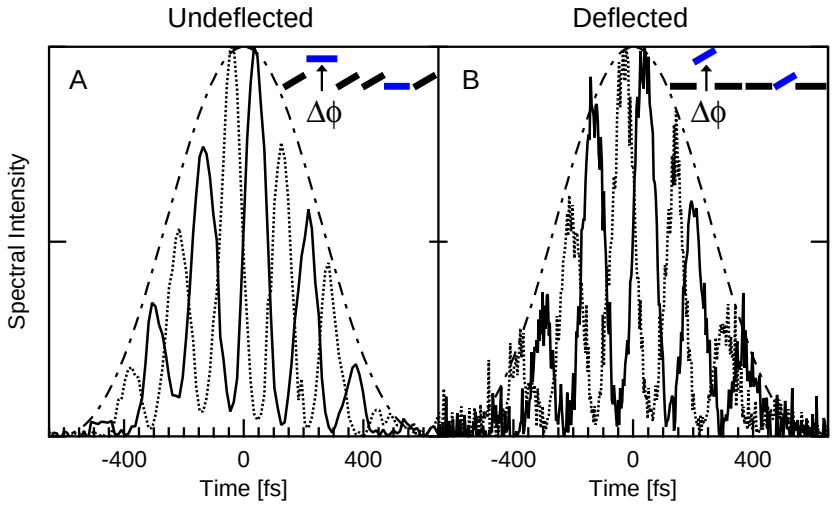

Fig. 3. Interference between two isolated spectral portions. Temporal cross-correlation traces revealing the effect of interferences between two isolated spectral portions for the undeflected (A) and the deflected (B) beam for a relative phase-shift $\Delta\phi$ of 0 (solid line) and π (dashed line). The blue elements in the symbolic representation indicate the two mirrors spectrally associated to the two interfering beam components. The theoretical temporal shaping-window allowed by the the setup is superimposed as a reference (dotted-dash line).

However, in complex and multi-elements set-ups, identifying the precise causes of spatial chirp and residual angular dispersion is not always trivial and - to our best knowledge - no active device has been proposed to date for its sharp correction.

We show here how our MEMS device can be used to introduce (and conversely correct) spatial chirp along one direction. In the central section of Fig. 4, we show the dependence of the spectral components of a femtosecond pulse after passing through the shaper with unactuated MEMS device. In the upper plot, one can observe that the spectrum is contained in a narrow $\sim$ 1 mm horizontal region, corresponding to the lateral dimension of the beam profile, indicating no or little presence of spatial chirp. The last observation is further confirmed by the inspection of the lower plot, showing the spectrally integrated intensity plotted as a function of the lateral position. On the contrary, in the lateral plots of Fig. 4, we show how we can easily introduce a linear spatial dependence of the wavelength components, by tilting each mirror element by an linearly increasing angle. To highlight the versatility of the approach, a spectral chirp is deliberately introduced in the two opposite directions and over an extremely large area spanning up to three millimeters. Clearly, such a procedure entails the appearance of a temporal chirp, appearing from the different optical paths traveled by the differently deflected beam portions. This temporal chirp can be compensated for by a combined piston actuation provided that the induced delay remains within the temporal shaping window [16]. Additionally, a similar procedure might be applied to design a specific spectral separation for processes highly sensitivity to frequency angular dispersion, like achromatic doubling [22] and spatio-temporal focusing [23, 24].

4. Conclusions

We have demonstrated the versatility of a new MEMS reflective shaper capable of phase-, amplitude-, and spatial-shaping over a broad wavelength range. Although the present study has

#142090 - $15.00 USD Received 3 Feb 2011; revised 17 Mar 2011; accepted 17 Mar 2011; published 5 Apr 2011

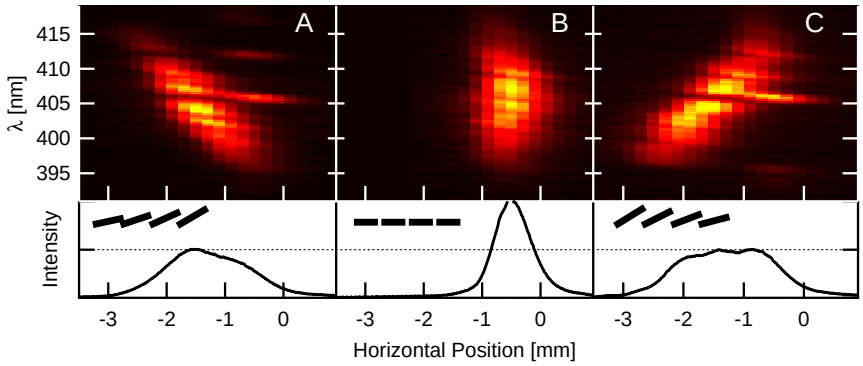

Fig. 4. Spatial chirp control. First row: spatial distribution along the horizontal axis of the pulse frequencies associated to three different angular MEMS patterns. Second row: corresponding spectrally integrated intensity. (A) tilt angle linearly increasing as a function of wavelength; (B) no tilting; (C) tilt angle linearly decreasing as a function of wavelength. The stripes out of the trend at 405 and 411 nm are due to the non-working mirrors, indicated by the red arrows in Fig. 1.

been realized on a chip with only 26 fully working mirrors, the potentialities of this technology can be readily perceived considering the present results and those previously obtained with a piston-only release of the MEMS chip [16]. To increase the working elements yield, a new production run addressing some critical fabrication aspects is planned.

Beyond the increasing range of applications of large bandwidth phase- and amplitude pulse-shaping, including coherent control, nonlinear imaging, laser micro-machining, we also propose the use of this device as active element for compensating for space-time and space-spectral coupling distortions [25–28] arising for instance upon propagation through dispersive and nonlinear elements.

Acknowledgments

We are grateful to Michel Moret, P.-A. Clerc, Michael Canonica, Peter Brühlmeier, Altatec AG, and the staff of the CSEM cleanroom facilities. We acknowledge the financial support of the Swiss National Science Foundation (SNSF) (contract 200020-124689/1), Swiss SER (COST MP0603), and Swiss NCCR "Quantum Photonics" and NCCR "MUST".

#142090 - $15.00 USD Received 3 Feb 2011; revised 17 Mar 2011; accepted 17 Mar 2011; published 5 Apr 2011